Understanding the drivers of near-surface winds in Adelie land

Cécile Davrinche[1], Anaïs Orsi[1,2], Cécile Agosta[1], Christoph Kittel[3], and Charles Amory[3]

[1]Laboratoire de Sciences du Climat et de l'Environnement, IPSL/CEA-CNRS-UVSQ UMR8212, Université Paris Saclay, Gif-sur-Yvette, France
[2]Department of Earth, Oceand and Atmospheric Sciences, The University of British Columbia, Vancouver, BC, Canada
[3]Institut des Géosciences de l'Environnement (IGE), Université Grenoble Alpes/CNRS/IRD/G-INP, Grenoble, France

Correspondence: Cécile Davrinche, cecile.davrinche@lsce.ipsl.fr

S1   Coordinate system:

We use two different sets of coordinates:

- (x_c, y_c, z_c) the regular cartesian coordinates

- (s_1, s_2, n), across the slope, downslope, and normal to the slope

5   In the following, physical quantities denoted by a star (*) correspond to quantities expressed in the (s_1, s_2, n) coordinates. The angle between z_c and n is α.
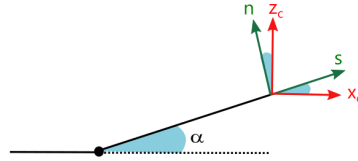
S2   Momentum balance

S2.1   Forces

10   In the following, P is the air pressure, and ρ is the air density.

The forces we are considering are:

- Pressure gradient force (**PGF**):

  - in (x_c, y_c, z_c): $\mathbf{PGF} = -\frac{1}{\rho} \cdot \boldsymbol{\nabla}(P) = -\frac{1}{\rho} \cdot (\frac{\partial P}{\partial x_c} \cdot x_c + \frac{\partial P}{\partial y_c} \cdot y_c + \frac{\partial P}{\partial z_c} \cdot z_c)$

  - in (s_1, s_2, n): $\mathbf{PGF}^* = -\frac{1}{\rho} \cdot (\frac{\partial P}{\partial s_1} \cdot s_1 + \frac{\partial P}{\partial s_2} \cdot s_2 + \frac{\partial P}{\partial n} \cdot n)$

15   - Buoyancy force (Gravity)

1

- in $(x_c, y_c \ z_c)$: Gravity $= g \cdot z_c$

- in (s_1, s_2, n): Gravity $= -g \cdot \sin(\alpha) \cdot s_1 - g \cdot \cos(\alpha) \cdot n$

- Coriolis force:

  - in $(x_c, y_c \ z_c)$: Coriolis $= f \cdot v \cdot x_c - f \cdot u \cdot y_c$, with (u, v) the wind speed coordinates in (x_c, y_c)

  - in (s, n): Coriolis $= f \cdot v^* \cdot s_1 - f \cdot u^* \cdot s_2$ with (u^*, v^*) the wind speed coordinates in (s_1, s_2)

- Turbulence and frictional forces : F

S2.2 Momentum balance

The momentum balance equation in (x_c, y_c, z_c) is:

$$\begin{cases} \frac{Dv}{Dt} = -\frac{1}{\rho} \cdot \frac{\partial P}{\partial x_c} + F_x \\ \frac{Dw}{Dt} = -\frac{1}{\rho} \cdot \frac{\partial P}{\partial z_c} - g + F_z \end{cases} \tag{1}$$

Since $\begin{cases} v = v^* \cdot \cos(\alpha) - w^* \sin(\alpha) \\ w = w^* \cdot \cos(\alpha) + v^* \sin(\alpha) \end{cases}$ And $\begin{cases} v^* = v \cdot \cos(\alpha) + w \cdot \sin(\alpha) \\ w^* = w \cdot \cos(\alpha) - v \cdot \sin(\alpha) \end{cases}$

$$\frac{Dv^*}{Dt} = \frac{Dv}{Dt} \cdot \cos(\alpha) + \frac{Dw}{Dt} \cdot \sin(\alpha) \tag{2}$$

Using: $\begin{cases} \frac{\partial}{\partial x_c} = \cos(\alpha) \cdot \frac{\partial}{\partial s} - \sin(\alpha) \cdot \frac{\partial}{\partial n} \\ \frac{\partial}{\partial z_c} = \sin(\alpha) \cdot \frac{\partial}{\partial s} + \cos(\alpha) \cdot \frac{\partial}{\partial n} \end{cases}$

We end up with the following equations in (s, n) coordinates:

$$\begin{cases} \frac{Dv^*}{Dt} = -\frac{1}{\rho} \frac{\partial P}{\partial s} - g \cdot \sin(\alpha) - f \cdot u^* + F_s \\ \frac{Dw^*}{Dt} = -\frac{1}{\rho} \frac{\partial P}{\partial n} - g \cdot \cos(\alpha) + F_n \end{cases} \tag{3}$$

We introduce P_r and P' as the background reference pressure and its perturbation, with $P = P_r + P'$. Both variables are in hydrostatic equilibrium. They depend on time, horizontal and vertical coordinates.

$$\begin{cases} \frac{Dv*}{Dt} = -\frac{1}{\rho} \frac{\partial P_r}{\partial s} - \frac{\rho_r}{\rho} \cdot g \cdot \sin(\alpha) - \frac{1}{\rho} \frac{\partial P'}{\partial s} - \frac{\rho'}{\rho} \cdot g \cdot \sin(\alpha) - f \cdot u^* + F_s \\ \frac{Dw*}{Dt} = -\frac{1}{\rho} \frac{\partial P_r}{\partial n} - \frac{\rho_r}{\rho} g \cdot \cos(\alpha) - \frac{1}{\rho} \frac{\partial P'}{\partial s} - \frac{\rho'}{\rho} \cdot g \cdot \cos(\alpha) + F_n \end{cases} \tag{4}$$

When the slope is small, we can approximate a hydrostatic equilibrium for w^*, meaning that:

$$
\begin{cases}
\frac{Dw^*}{Dt} \approx 0 \\[2mm]
\frac{\partial P}{\partial n} = -\rho \cdot g \cdot \cos(\alpha)
\end{cases}
\tag{5}
$$

As P_r and P' are in hydrostatic equilibrium as well,

$$
\begin{cases}
\frac{\partial P_r}{\partial n} = -\rho_r \cdot g \cdot \cos(\alpha) \\[2mm]
\frac{\partial P'}{\partial n} = -\rho' \cdot g \cdot \cos(\alpha)
\end{cases}
\tag{6}
$$

We define ρ_{r0} and P_{r0} a constant density and a constant pressure in the horizontal dimensions which value remain close to ρ and P. We integrate Eq. 6 with respect to the n coordinate and we divide by ρ_{r0}:

$$
\frac{1}{\rho_{r0}} \int_n^h \frac{\partial P'}{\partial n} dn = -\frac{g \cdot \cos(\alpha)}{\rho_{r0}} \int_n^h \rho' dn
\tag{7}
$$

where h is a height above which $P = P_r$ and $P' = 0$. Therefore:

$$
\frac{1}{\rho_{r0}} P'(n) = -\frac{g \cdot \cos(\alpha)}{\rho_{r0}} \int_n^h \rho' dn
\tag{8}
$$

Introducing the potential temperature $\theta = (\frac{P}{\rho R})^{1-\kappa}(P_0)^\kappa$, with $P_0 = 1000$ hPa, we use the logarithmic derivative:

$$
\frac{\Delta(\theta)}{\theta} = (1-\kappa)\frac{\Delta(P)}{P} - \frac{\Delta(\rho)}{\rho}
\tag{9}
$$

In the case of a shallow circulation:

$$
\frac{\Delta(\theta)}{\theta} = -\frac{\Delta(\rho)}{\rho}
\tag{10}
$$

We define θ_{r0} as the potential temperature associated with ρ_{r0} and P_{r0}:

$$
\implies \frac{1}{\rho_{r0}} P' = -\frac{g \cdot \cos(\alpha)}{\theta_{r0}} \int_n^h \theta' dn
\tag{11}
$$

We derive the previous equation with respect to s:

$$
\frac{1}{\rho_{r0}} \frac{\partial P'}{\partial s} = -\frac{g \cdot \cos(\alpha)}{\theta_{r0}} \int_n^h \frac{\partial \theta'}{\partial s} dn
\tag{12}
$$

As ρ_{r0} remains close to ρ:

$$60 \quad \frac{1}{\rho}\frac{\partial P'}{\partial s} \approx -\frac{g\cdot\cos(\alpha)}{\theta_{r0}}\int_n^h \frac{\partial\theta'}{\partial s}dn \tag{13}$$

Using the different developments and simplifications that we have made, we can rewrite Eq. (4) for the downslope coordinate:

$$\boxed{\frac{Dv^*}{Dt} = \underbrace{-\frac{1}{\rho}[\frac{\partial P_r}{\partial s}+\rho_r\cdot g\cdot\sin(\alpha)]}_{\text{Large-scale}}+\underbrace{\frac{g\cdot\cos(\alpha)}{\theta_{r0}}\int_n^h\frac{\partial\theta'}{\partial s}dn}_{\text{Thermal wind}}-\underbrace{\frac{\rho'}{\rho}\cdot g\cdot\sin(\alpha)}_{\text{Katabatic}}-\underbrace{f\cdot u^*}_{\text{Coriolis}}+F_s} \tag{14}$$

Thermal wind **THWD** is then computed as follows:

$$\boxed{\textbf{THWD} = \frac{g\cdot\cos(\alpha)}{\theta_{r0}}\int_n^h\frac{\partial\theta'}{\partial s}dn} \tag{15}$$

65 Eq. (14) has been derived in what we call "sigma coordinates". From here we are unable to compute the large-scale acceleration because we don't have access to p_r or to ρ_r. We will need another formula for this term.

From (1) and (3):

$$\frac{\partial P_r}{\partial s}+\rho_r\cdot g\cdot\sin(\alpha) \approx -\frac{1}{\rho}\frac{\partial P_r}{\partial x_c} \tag{16}$$

Let v_r be a wind speed such that P_r and v_r are in thermal-wind balance.

$$70 \quad -\frac{1}{\rho}\frac{\partial P_r}{\partial x_c} = -f.v_r \tag{17}$$

Using the chain rule:

$$v_r = -\frac{1}{\rho f}\frac{\partial P_r}{\partial z_c}(\frac{\partial z_c}{\partial x_c})|_{P_r} \tag{18}$$

Thus, with Φ_r the geopotential associated to P_r

$$v_r = -\frac{\rho_r g}{\rho f}(\frac{\partial z_c}{\partial x_c})|_{P_r} = -\frac{\rho_r g}{\rho f}(\frac{\partial\Phi_r}{\partial x_c}) \approx -\frac{1}{f}(\frac{\partial\Phi_r}{\partial x_c}) \tag{19}$$

75 Using the definition of the potential temperature and the derivative with respect to P:

$$\frac{\partial v_r}{\partial P} = -\frac{R}{fP_r}(\frac{\partial T_r}{\partial x_c})|_{P_r} \tag{20}$$

$$P_r\frac{\partial v_r}{\partial P} = -\frac{R}{f}(\frac{P}{P_0})^{\frac{R_d}{C_p}}(\frac{\partial\theta_r}{\partial x_c})|_{P_r} \tag{21}$$

4

If P and P_r are similar enough, which is a huge hypothesis, we can write:

$$P\frac{\partial v_r}{\partial P} = -\frac{R}{f}(\frac{P}{P_0})^{\frac{R_d}{C_p}}(\frac{\partial \theta_r}{\partial x_c})|_P \tag{22}$$

And it leads us to this expression:

$$\boxed{\frac{\partial v_r}{\partial ln(P)} = -\frac{R}{f}(\frac{P}{P_0})^{\frac{R_d}{C_p}}(\frac{\partial \theta_r}{\partial x_c})|_P} \tag{23}$$

As $\theta_r(x,y,z) = \tau_0(x,y) + \gamma_0(x,y) \cdot z_c$ (see article), with z_c the altitude above ground level, we obtain:

$$\frac{\partial \theta_r}{\partial x_c}|_P = \frac{\partial \tau_0}{\partial x_c} + \frac{\partial \gamma_0}{\partial x_c} \cdot z_c + \gamma_0 \cdot \frac{\partial z_c}{\partial x_c}|_P \tag{24}$$

At 500 hPa, on average, $\frac{\partial \gamma_0}{\partial x_c} \cdot z_c \approx 10^{-2}$ and $\frac{\partial z_c}{\partial x_c} \cdot \gamma_0 \approx 10^{-4}$. The following simplification is thus made to compute v_r:

$$\boxed{\frac{\partial \theta_r}{\partial x_c}|_P = \frac{\partial \tau_0}{\partial x_c} + \frac{\partial \gamma_0}{\partial x_c} \cdot z_c} \tag{25}$$

S3   Choice of a lower boundary H_{min} for linear interpolation of θ

In order to accurately select H_{min}, it is crucial to identify the minimum height at which the vertical gradient of potential temperature ($\frac{\partial \theta}{\partial z_c}$) diverges from its value in the linear section (γ_{linear}). We consider $\gamma_{350-500}$ (the value of the vertical gradient of potential temperature computed between 350 and 500 hPa), to be an initial guess of γ_{linear} and define H_{min}, as the height under which $|\frac{\partial \theta}{\partial z_c} - \gamma_{350-500}| > Thresh_{\frac{\partial \theta}{\partial z_c}}$.

We chose to express this threshold as a proportion of the vertical gradient of potential temperature in the linear section: $Thresh_{\frac{\partial \theta}{\partial z_c}} =$ N*$\gamma_{350-500}$, taking into account the fact that slight variations around a linear profile are common. In order to determine the ideal multiplier N of $\gamma_{350-500}$, we computed H_{min} for a range of N. If N is too small, then H_{min} is too high in the atmosphere, and a value of H_{min} above Z_{500} is unacceptable: There would be no difference between γ_{linear} and $\gamma_{350-500}$. If N is too large, , the interpolation is likely to extend excessively close to the surface (H_{min} < 100 m agl). As we assume the surface processes to always be active under 100 m agl, in these cases, H_{min} is forced to this value. In Figure S1, we show in yellow the number of cases when $H_{min} > Z_{500}$, and in green the number of cases when H_{min} < 100 m agl, as a function of N. The ideal N is when both these metrics are minimized, and in this range, we chose the smallest N.

The minimum value of the multiplier of $\gamma_{350-500}$ for which H_{min} is always smaller than Z_{500} (red line on Fig. S1) is a good indicator of the optimal value for the multiplier of $\gamma_{350-500}$. This value is comprised between $2 \cdot \gamma_{350-500}$ for DC and $5 \cdot \gamma_{350-500}$ for the other stations.

Additionally, we show on Figure S2 that the computation of θ_0 is only weakly sensitive to a reasonable choice of N: there is no substantial difference between the background potential temperature computed with 2, 4 or 6 $\gamma_{350-500}$, as shown for D17 at 7 m agl. In the end, we used a single value of N=4, which is an intermediate value between the optimal multiplier at D17 and DC, and demonstrated that the computation of θ_0 is robust to this choice.
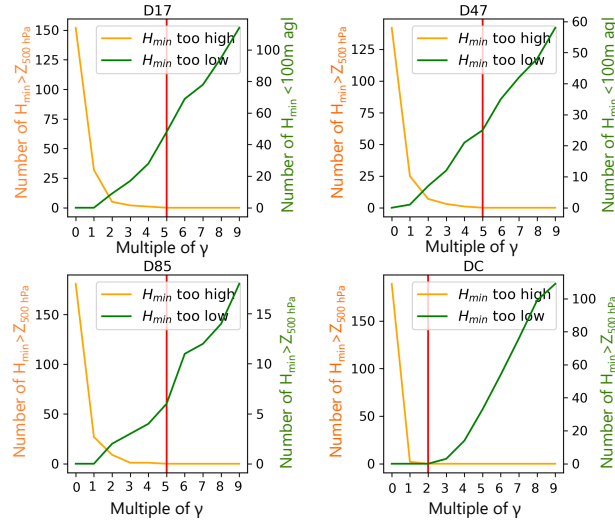
Fig. S1. Number of timesteps for which H_{min} is greater than Z_{500} (orange line) and number of timesteps for which H_{min} is smaller than 100 m agl and forced to 100 m agl in July 2010 at 4 different stations as function of N. N is the multiplier of $\gamma_{350-500}$, defined in the paragraph S3. (a) D17, (b) D47, (c) D85, (d) DC. The red line indicates the minimum value of the multiplier of $\gamma_{350-500}$ for which H_{min} is always smaller than Z_{500}
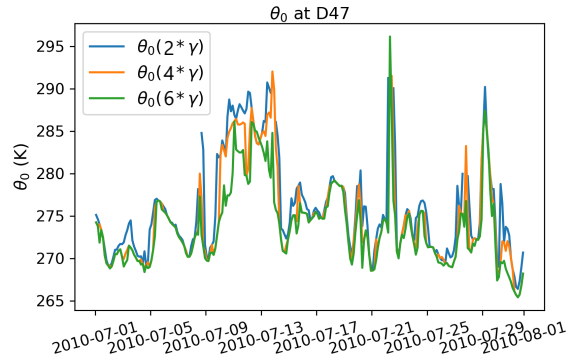

Fig. S2. θ_0 (background potential temperature) computed at D47, at surface level (7 m agl) for July 2010, using $2 \cdot \gamma_{350-500}$ (blue line), $4 \cdot \gamma_{350-500}$ (orange line) and $6 \cdot \gamma_{350-500}$ (green line) threshold for determining H_{min}.

S4   Computation of H_{min} using a second order derivative method

Mathematically, the 1st derivative of a linear curve is a constant (the slope), while its 2nd derivative is zero. Thus, in the linear part of the vertical profile of potential temperature, the 1st derivative is a constant (γ) and the 2nd derivative is zero. We chose to define the boundary of the linear profile of θ as the height H_{min} under which $|\frac{\partial \theta}{\partial z_c} - \gamma_{350-500}| > 4 * \gamma_{350-500hPa}$.

A second method to determine H_{min} would be to use a threshold on the second vertical derivative: H_{min} is the height under which $\frac{\partial^2 \theta}{\partial z^2} > Thresh_{\frac{\partial^2 \theta}{\partial z^2}}$.

We show on Figure S3 the values for H_{min} using a threshold of $10^{-4} K/m^2$ or $10^{-3} K/m^2$. We find that using a thresold of $10^{-4} K/m^2$ leads to a very similar estimation of θ_0 than the first method with N=4, with a difference smaller than 0.5% is most of Antarctica, and up to 3% in the Weddell sea (Figure S4) .

Although this is also a valid method, there are several important caveats to using a thresold on the second derivative $Thresh_{\frac{\partial^2 \theta}{\partial z^2}}$:

- The vertical discretization is different close to the ground than higher up in the atmosphere, meaning that there can be some artificial discontinuities in the 2nd derivative

- The 2nd derivative in the "linear part" is not exactly zero, because the profile is not perfectly linear. Therefore, one must be carefull to define $Thresh_{\frac{\partial^2 \theta}{\partial z^2}}$ big enough, so that it does not result in an artificially high value of $H_{\frac{\partial^2 \theta}{\partial z^2}}$.

- $Thresh_{\frac{\partial^2 \theta}{\partial z^2}}$ cannot be too big, because otherwise, we might miss the deviation and interpolate too low.

- $Thresh_{\frac{\partial^2 \theta}{\partial z^2}}$ must be valid for all 3-hourly time step and grid point

Therefore, a fixed threshold for the 2nd derivative does not appear to provide any advantage over using a threshold on the 1st derivative: Both include a somewhat subjective choice of the threshold, although we show here that the specific method used is not critical, and that we can reliably estimate θ_0 with any method, and a reasonable choice of the threshold (Figures S3 and S2)
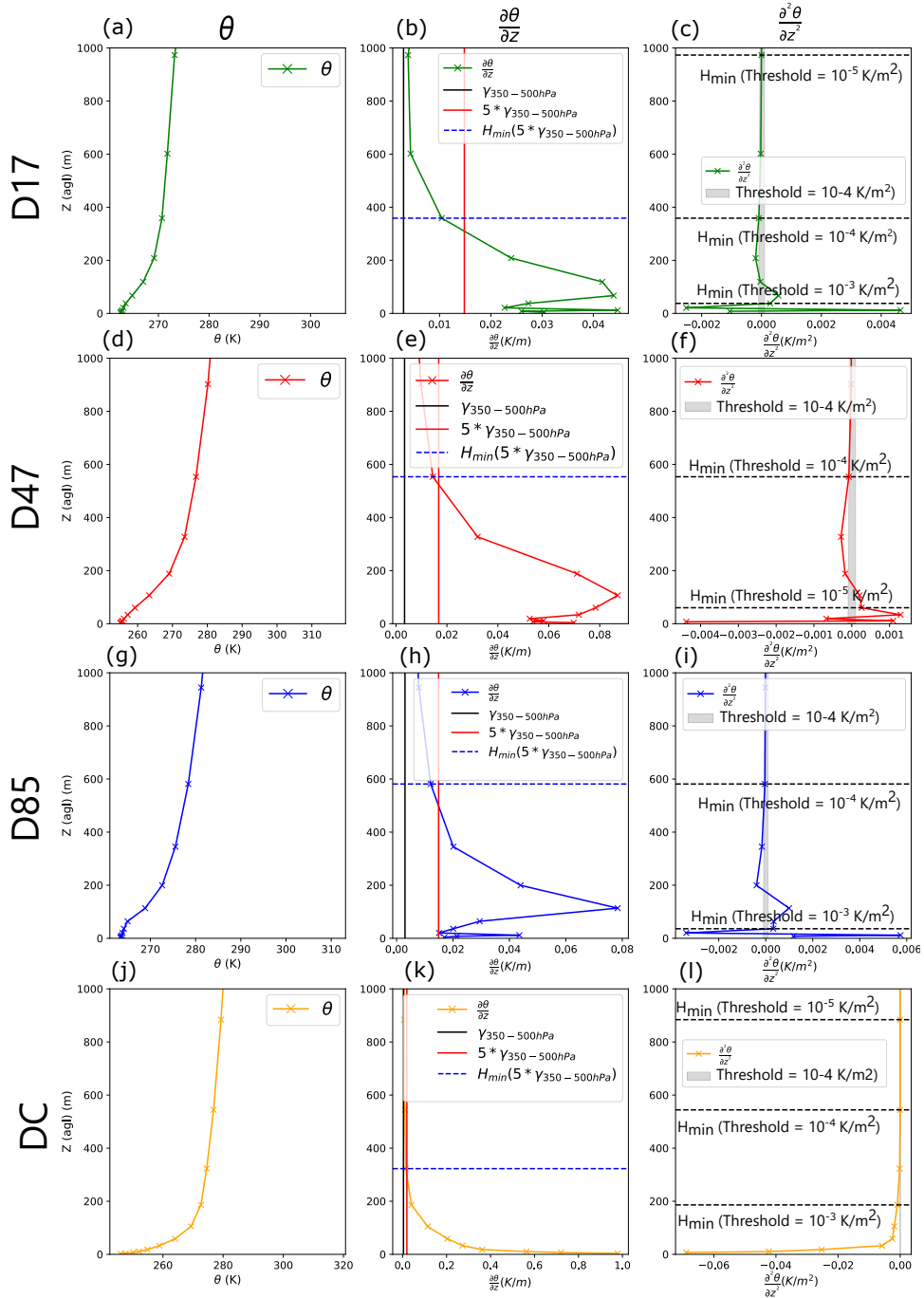
S5   Supplementary Figures

Fig. S3. Vertical mean July 2018 profiles of (a, d, g, j) θ, (b, e, h, k) $\frac{\partial \theta}{\partial z}$ and (c, f, i, l) $\frac{\partial^2 \theta}{\partial z^2}$ at D17, D47, 85 and DC (from top to bottom). The blue dotted lines in the middle panels indicate the minimum height for interpolation of θ_0 computed using the 1st order vertical derivative method described in the manuscript. The black dashed lines in the right panels indicate the minimum height for interpolation of θ_0 computed using a 2nd order derivative method for three different values of $Thresh_{\frac{\partial^2 \theta}{\partial z^2}}$

Mean July 2018
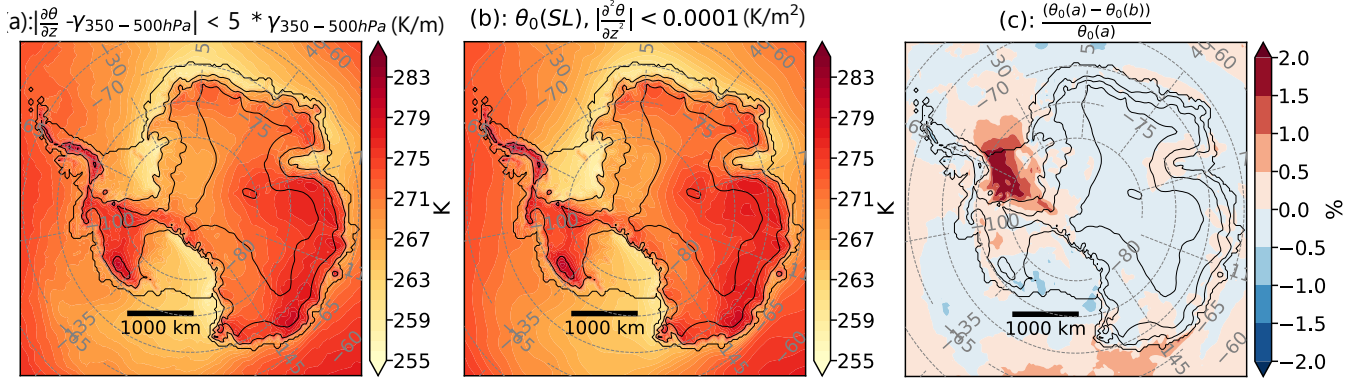
Fig. S4. θ_0 at surface level computed computed (a) using the method (described in the manuscript) based on the 1st order vertical derivative (b) using a method based on the 2nd order vertical derivative, with a threshold $\frac{\partial^2 \theta}{\partial z^2} = 0.0001 K/m^2$ (c) difference between θ_0 computed using method (a) and (b)
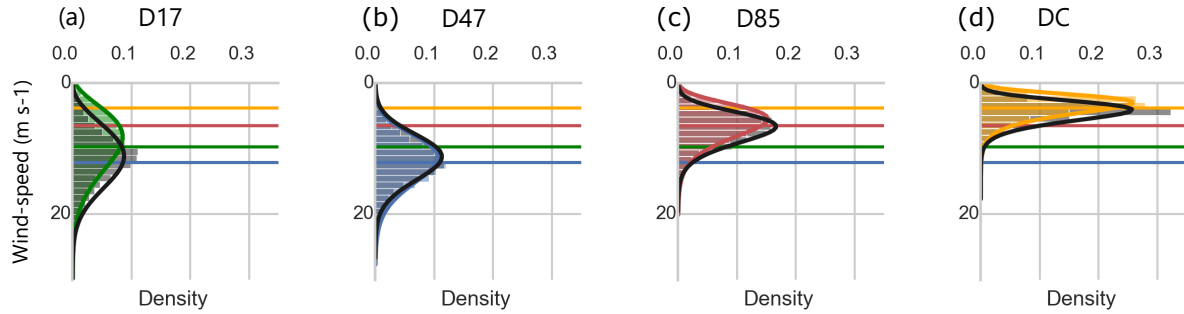

Fig. S5. Distributions of July 2010 2m MAR (black distributions) and observed (colored distributions) wind-speed at (a) D17 (b) D47 (c) D85 (d) DC. The black and colored fits correspond to the Weibull fit respectively for MAR and for the observations. The four horizontal lines indicate the mean wind-speed of each station.

Station	Shape parameter		Scale parameter	
	κ_{obs}	κ_{MAR}	λ_{obs}	λ_{MAR}
D17	1.49	2.72	10.04	12.84
D47	7.14	4.42	88.96	28.72
D85	1.46	3.03	4.80	16.47
DC	1.05	1.83	1.62	4.40

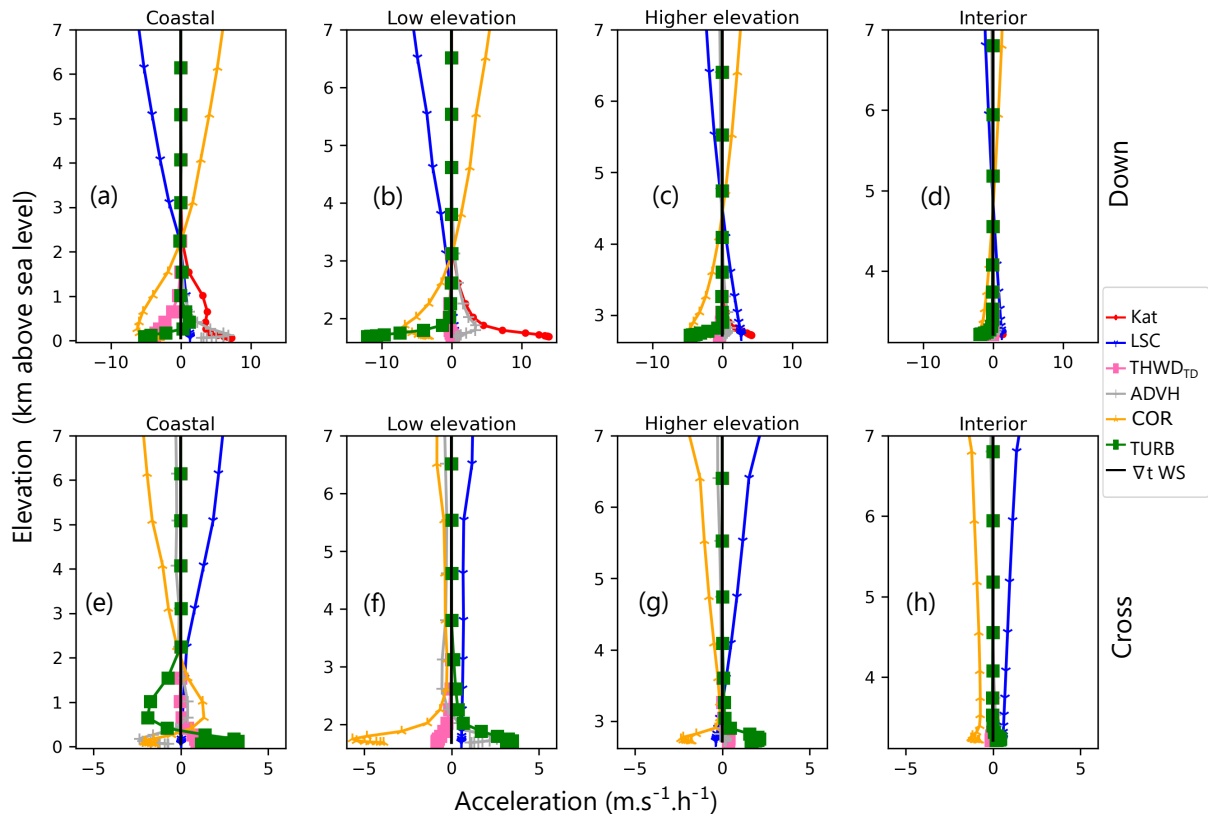**Table S1.** Weibull parameters associated with the distributions displayed on Fig. S3

9

Fig. S6. Vertical profiles averaged over July 2010-2020 of each downslope acceleration (top panel, the x-axis extends from -15 to 15 $m\,s^{-1}\,h^{-1}$) and cross-slope accelerations (bottom panel, the x-axis extends from -6 to 6 $m\,s^{-1}\,h^{-1}$) for the 4 zones on the transect.
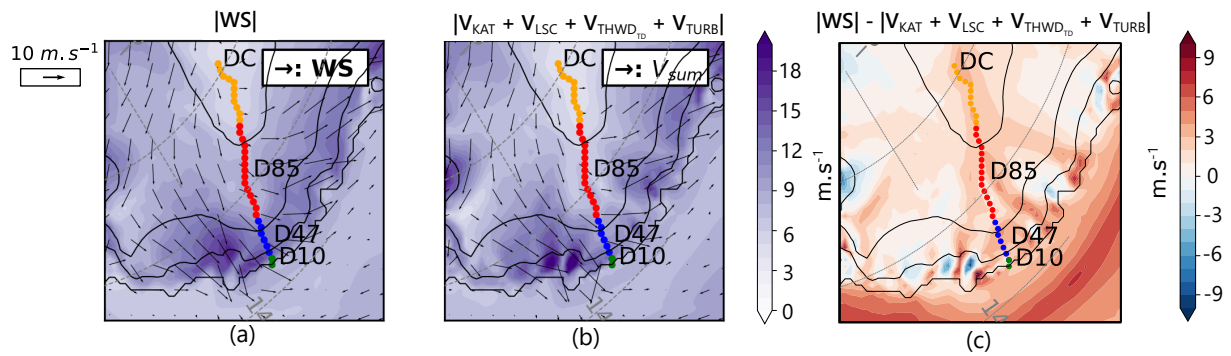
Fig. S7. (a) Mean July 2010-2020 total wind speed, (b) wind speed associated to the sum of dominant terms, i.e. katabatic, large-scale, thermal wind and turbulent acceleration (c) Difference between (a) and (b) at surface level ($\sim$7 m agl), computed with 3-hourly MAR outputs.
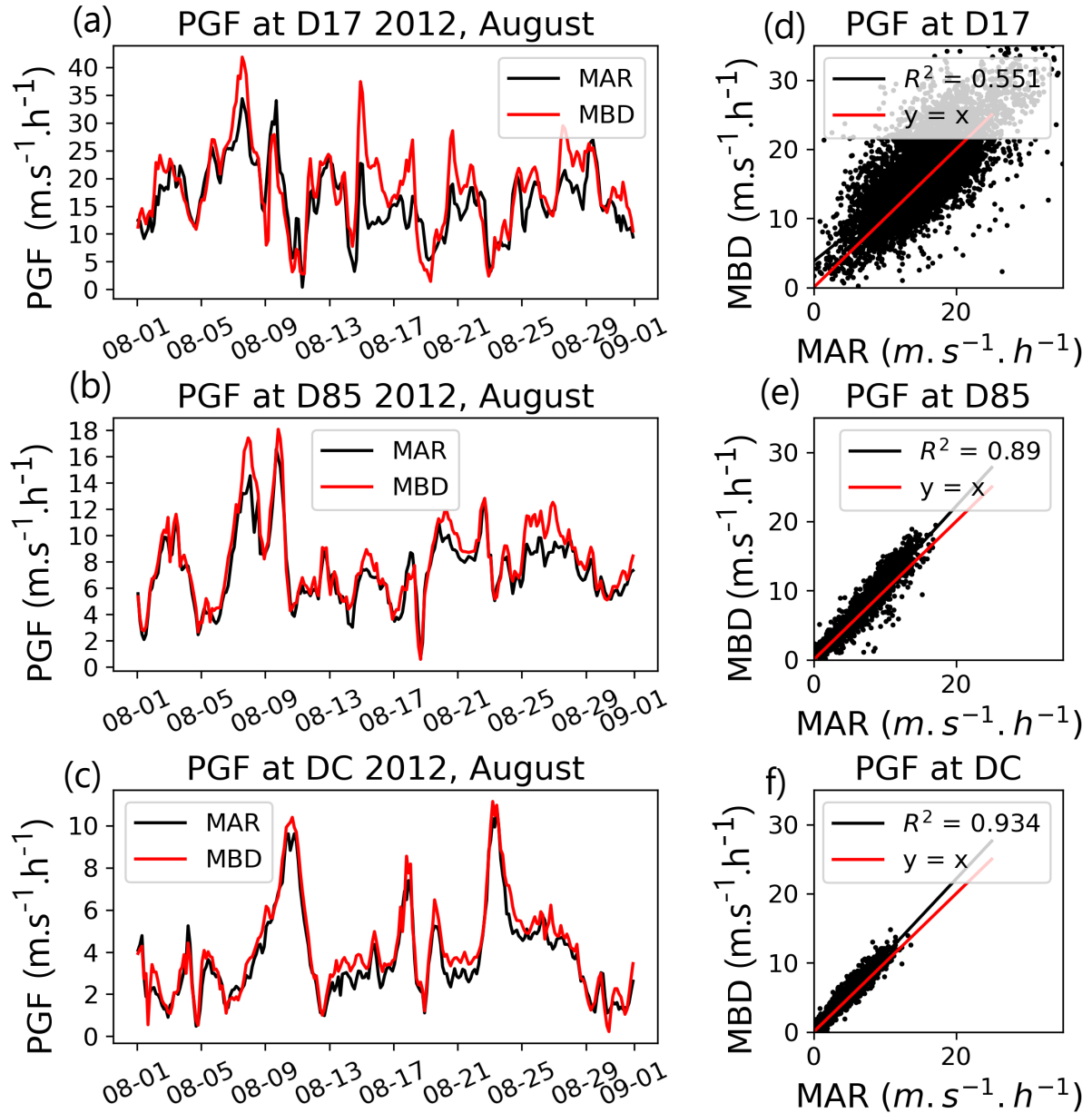
Fig. S8. Comparison of MAR PGF output with our MBD PGF at the surface at D17 (a, d), D85 (b, e) and DC (c, f). Left panel (a, b, c): 3-hourly time serie comparison of MAR PGF versus MBD PGF for a winter month (August 2012). Right panel (d, e, f): scatter plot of MAR PGF versus MBD PGF for the months of winter (June, July, August) 2010-2020.
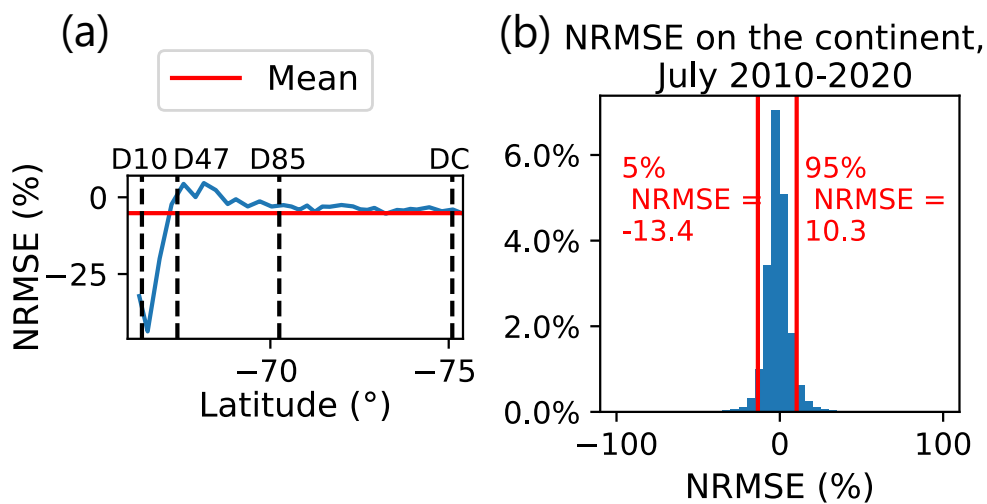
Fig. S9. (a) Normalized root mean square error (NRMSE) computed for the PGF (July 2010-2020) along the transect, between MAR (online) and our MBD method, at 7 m agl. The red line indicates the average NRMSE value on the transect. (b) Histogram of the NRMSE on the continent. The two vertical red lines represent the 5% and 95% percentiles of the total distribution for July 2010-2020.
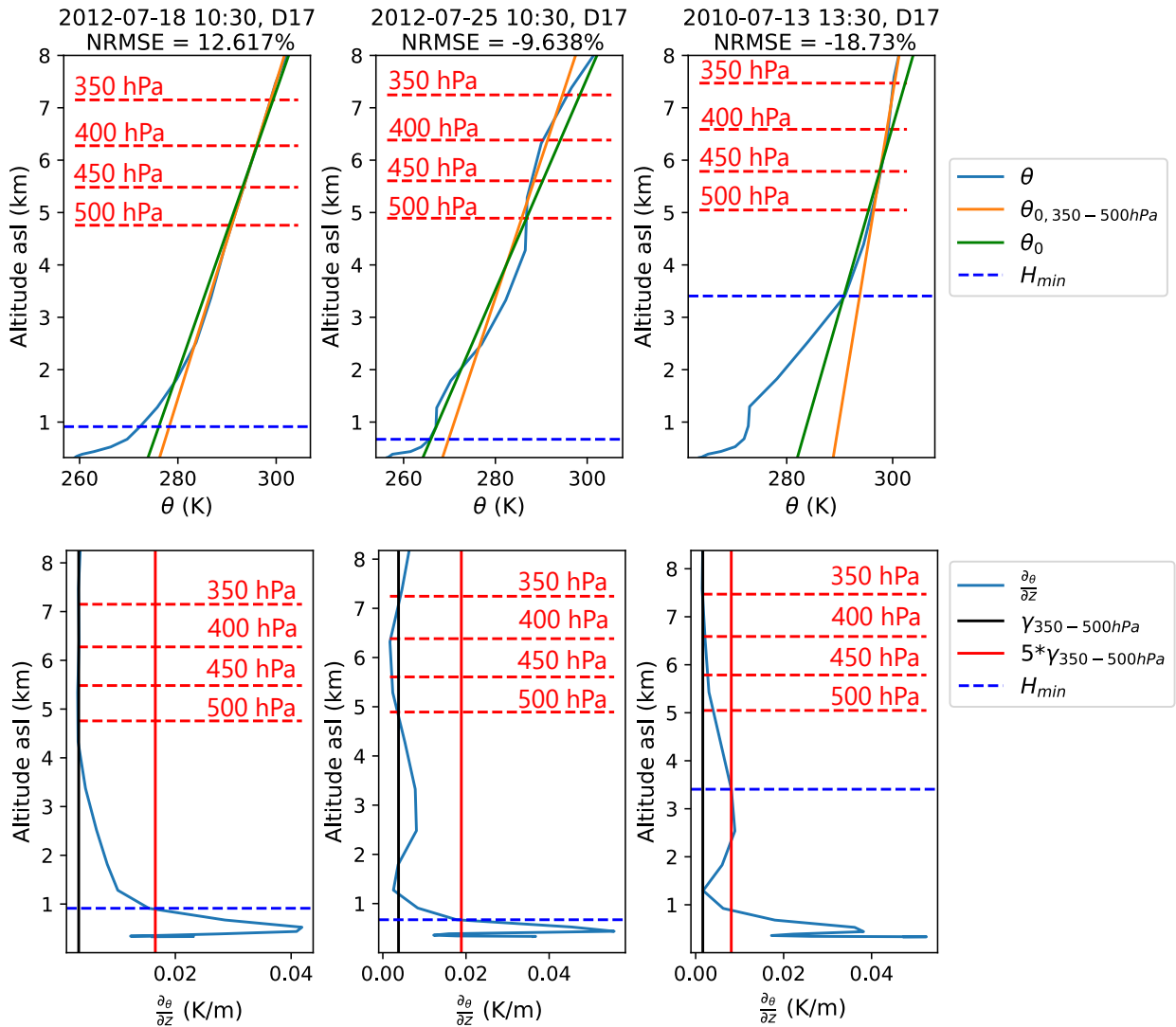
Fig. S10. Examples of profiles exhibiting a high Normalized Root Mean Square Error (NRMSE) between the native MAR PGF and our MBD PGF at D17. (a), (b) and (c): vertical profile of potential temperature (blue solid line), background potential temperature computed using the first order derivative (green solid line) computed by interpolating the potential temperature profile between 350 and 500 hPa (orange line). (d), (e), (f): vertical profiles of the first order derivative of potential temperature (blue solid line), value of $\frac{\partial \theta}{\partial z}$ computed between 350 and 500 hPa (black solid line), threshold value of $5 \times \gamma_{350-500}$ below which we consider the vertical potential temperature profile to be no longer quasi-linear (red solid line). For both panels, red dashed lines indicate pressure levels of 500 hPa, 450 hPa, 400 hPa and 350 hPa and blue dashed lines indicate the minimun height H_{min} for the interpolation of the background potential temperature. Profile (a) is a typical case where there is no abrupt increase in the vertical derivative of potential temperature at the top of the inversion layer. Profile (b) is a typical case of intrusion of an air-mass (characterized by a non strictly monotonous profile of potential temperature) and profile (c) is a typical case exhibiting a secondary linear section with a different slope under 500 hPa.
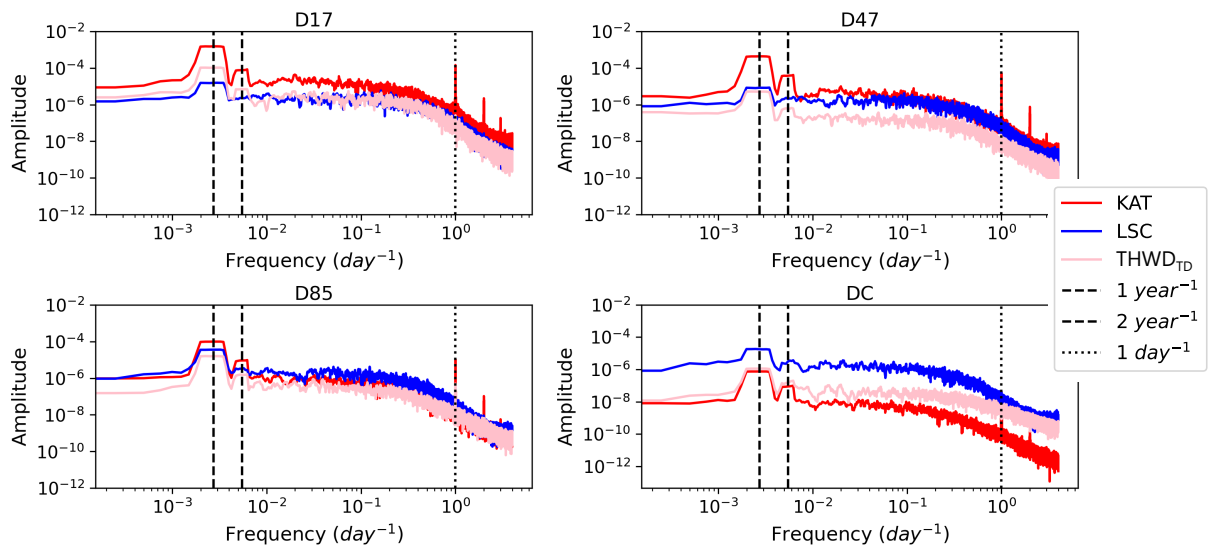
Fig. S11. Fourier transform of katabatic (red), large-scale (blue) and thermal-wind (pink) accelerations for the 4 stations on the transect.